

Electronic Structure of Trigonal-Planar Transition-Metal–Imido Complexes: Spin-State Energetics, Spin-Density Profiles, and the Remarkable Performance of the OLYP Functional†

Jeanet Conradie‡,§ and Abhik Ghosh*,‡

Center for Theoretical and Computational Chemistry, Department of Chemistry, University of Tromsø, N-9037 Tromsø, Norway, and Department of Chemistry, University of the Free State, 9300 Bloemfontein, Republic of South Africa

Received November 16, 2006

Abstract: We have carried out a detailed multifunctional density functional theory study of first-row transition-metal (Cr to Cu) β -diketiminato (“nacnac”) imido and oxo complexes. All the complexes studied exhibit essentially the same d-orbital energy ordering, which is $a_1(d_{x^2-z^2}) \leq a_2(d_{xy}) \leq a_1(d_{yz}) < b_2(d_{yz}) < b_1(d_{xz})$, where the metal–imido vector is identified with the z axis and metal–N₃ plane is identified with the xz plane. A curious aspect of this orbital ordering is that the metal $d_{x^2-z^2}$ orbital, one of whose lobes points directly at the imido nitrogen, is considerably lower in energy than the d_π orbitals. We have determined that the remarkable stability of the d_σ -type orbitals owes largely to the way these orbitals hybridize or “shape-shift” as a result of the absence of ligands trans or equatorial with respect to the imido (or oxo) group. Of the many functionals examined, OLYP and OPBE, based on the Handy–Cohen OPTX exchange functional, appear to provide the best overall description of the spin-state energetics of the various complexes. In particular, these two functionals predict an $S = 3/2$ ground state for Fe(III) nacnac imido complexes and an $S = 0$ ground state for Co(III) nacnac imido complexes, as observed experimentally. In contrast, classic pure functionals such as PW91 predict $S = 1/2$ ground states or at best equienergetic $S = 1/2$ and $S = 3/2$ states for the Fe(III) imido complexes, while hybrid functionals such as B3LYP and O3LYP predict $S = 1$ or 2 ground states for the Co(III) nacnac imido complexes.

Introduction

Multiply bonded metal–ligand units are a subject of enduring interest in chemistry.¹ In part, this interest stems from the relevance of such units as mimics of enzymatic iron–oxo intermediates.^{2,3} In addition, transition-metal oxo, imido,^{4,5} nitrido, phosphinidene and phosphido complexes undergo a variety of synthetically useful atom- and group-transfer reactions.⁶ Not surprisingly, inorganic chemists are continu-

ally driven to create new multiply bonded metal–ligand entities, while theoreticians rush to elucidate their electronic structures. Interestingly, not long ago, middle and late transition-metal oxo and imido complexes were thought to be inevitably unstable and inaccessible, because of energetically costly metal(d_π)–ligand(p_π) antibonding interactions.⁷ However, our conception of the field has changed dramatically in recent years; thus, quite a few low-coordinate middle and late transition-metal imido complexes have been synthesized and structurally characterized.^{5,8–19} Although density functional theory (DFT) calculations have accompanied a number of these synthetic studies, a comprehensive, comparative electronic-structural perspective of the different

† Dedicated to Dennis R. Salahub on the occasion of his 60th birthday.

* Corresponding author e-mail: abhik@chem.uit.no.

‡ University of Tromsø.

§ University of the Free State.

complexes has yet to emerge, which is what we sought to develop in our laboratory. Accordingly, we will present here a systematic account of DFT calculations, employing a variety of exchange-correlation functionals, on trigonal-planar (β -diketiminato)M(NR) complexes, where M = Cr(III), Mn(III), Fe(III), Fe(IV), Co(III), Ni(III), and Cu(III) and R = alkyl or aryl. Warren and co-workers have synthesized and structurally characterized close experimental analogues of two of these complexes, namely, Co(III) ($S = 0$)²⁰ and Ni(III) ($S = 1/2$).²¹ Some of the specific issues that we sought to address in this study are as follows.

Although DFT calculations have provided a “first-order” electronic description of certain of the above complexes,^{19–21} we remained particularly intrigued by a key aspect of the bonding. Several of these complexes have a low-energy, single or doubly occupied metal($d_{x^2-z^2}$)–imido(p_σ) σ -antibonding molecular orbital (MO) that is significantly lower in energy than the two d_π – p_π antibonding MOs. However, there is little comment in the literature as to why a σ -antibonding MO should fill preferentially, relative to the π -antibonding MOs. Is this a special feature of the imido ligand? To investigate, we have compared the above-mentioned imido complexes with a full set of the corresponding oxo species, which have yet to be experimentally observed. We will see that the d-orbital ordering is largely determined by the trigonal-planar stereochemistry of the metal center.

Another aspect of the bonding we will focus on involves the spin-density profiles of the complexes. So far, there is little information in the literature on the spin-density distributions of the Fe(III) and Ni(III) imido complexes, for which DFT calculations have been reported.^{19–21} Here, we provide detailed information, partly via high-quality spin-density plots, on the spin-density profiles of all the open-shell species studied. By indicating how the spin density partitions itself between the metal and the ligands, this information affords a remarkably useful tool for visualizing and quantifying the nature of metal–ligand covalent bonding in open-shell coordination complexes.^{22,23}

Perhaps the key contribution of this study is toward elucidating the spin-state energetics²⁴ of the various trigonal-planar imido complexes. Already, the literature raises a number of intriguing questions. For example, an Fe(III) imido complex apparently exhibits an unusual intermediate-spin $S = 3/2$ ground state,¹⁹ while the analogous Co(III) complex is $S = 0$.²⁰ How much higher in energy are the alternative spin states? We have posed similar questions for the other imido complexes as well. In this connection, our calculations on the hypothetical oxo analogues of the imido complexes have also proved very insightful. As expected, significant differences exist between the energy spacings of the valence MOs of the imido and oxo complexes. We will see that in certain cases analogous imido and oxo complexes are even predicted to exhibit different ground states.

Intimately associated with the question of transition-metal spin-state energetics is the issue of how accurately we can compute them.^{24–26} As far as DFT is concerned, it is fair to say that we are still in the early stages of providing a

comprehensive answer to this question. In our experience, traditional pure functionals such as PW91 tend to favor low-spin, more-covalent states, while hybrid functionals such as B3LYP behave oppositely.^{24,26} In this study, we have carried out full geometry optimizations with two different functionals—PW91 and OLYP—as well as single-point energy calculations with a large variety of functionals, both pure and hybrid. An important conclusion to emerge from this large volume of data is that some of the newer “pure” functionals OLYP and OPBE, based on Handy and Cohen’s OPTX exchange functional,²⁷ may be among the best, from the point of view of transition-metal spin-state energetics.

Methods

All species studied were optimized with the PW91²⁸ and OLYP²⁷ generalized gradient approximations, triple- ζ plus polarization Slater-type orbital basis sets, and a fine mesh for numerical integration of the matrix elements, as implemented in the ADF 2005²⁹ program system. In addition, we also carried out single-point noniterative post-self-consistent field (SCF) calculations with a variety of pure and hybrid functionals, namely, BLYP,^{30,31} BP86,^{32,33} OPBE,^{27,34,35} XLYP,³⁶ B3LYP(VWN5),^{37–39} O3LYP(VWN5),^{27,38} and X3LYP(VWN5).³⁶ Unless otherwise indicated, the VWN functional was used as the local part of all of the above functionals. In general, for all the species studied, the calculated $\langle S^2 \rangle$ values were in excellent agreement with the theoretically expected values.

Results and Discussion

A. A Basic Description of the Bonding. Before discussing the bonding in the imido complexes, it might be useful to start with a qualitative MO picture of an electronically “simpler” β -diketiminato complex, (nacnac)NiL, where nacnac[−] is the anion of 2,4-bis(2,6-dimethylphenylimido)pentane and L is a relatively weak, innocent ligand such as chloride. Such a picture, already available from earlier work in this field,^{19,20,21,40,41} is presented in Figure 1. Under C_{2v} symmetry, the five d orbitals transform as $2a_1$, a_2 , b_1 , and b_2 . Both d_σ orbitals (relative to the metal–L linkage) transform as a_1 and are denoted as a_{1-1} (d_{y^2}) and a_{1-2} ($d_{x^2-z^2}$), where the metal–L axis defines the z direction, while the two d_π orbitals transform as b_1 and b_2 and the d_δ orbital as a_2 . The b_1 -symmetry M(d_π)–imido(p_π) antibonding MO has the highest orbital energy of all the metal d-based MOs, a feature that persists in the metal–imido complexes as well. The high energy of this MO also owes significantly to σ -antibonding interactions with the nacnac ligand, as depicted in Figure 1.

In this work, we have modeled the experimentally known 1-adamantylimido^{19–21} complexes as NMe and NPh complexes; the latter has the advantage of capturing the full C_{2v}

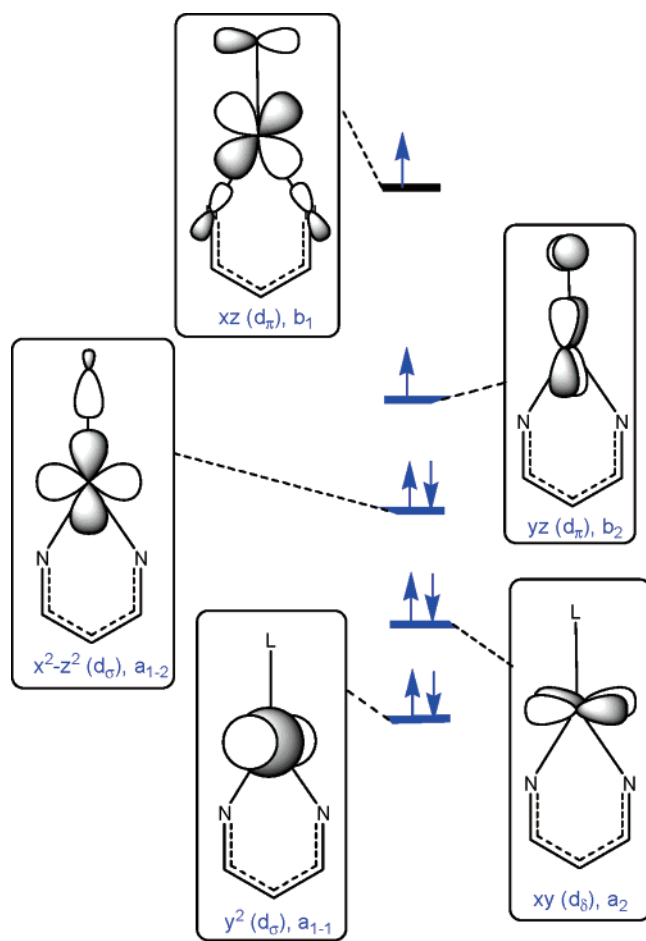


Figure 1. Qualitative MO diagram for a typical β -diketiminato complex, (nacnac)NiL, where L is a relatively weak, innocent ligand such as chloride. The d_σ , d_π , and d_δ descriptions are relative to the M–L bond.

symmetry of the bonding problem. Extensive symmetry-unconstrained optimizations confirmed that the C_s and C_{2v} point group symmetries were appropriate for nearly all the NMe and NPh complexes, respectively. In addition, we found that the phenyl group in the NPh moiety generally exhibits a distinct energetic preference for being coplanar with the metal–N₃ moiety. Figure 2 presents PW91 MO energy-level diagrams for four of the NPh complexes, namely, Fe(III) ($S = 3/2$), Co(III) ($S = 0$), Ni(III) ($S = 1/2$), and Cu(III) ($S = 1$), while Table 1 details the atomic compositions of the five primarily d-type MOs. Note from Figure 2 is that all four compounds exhibit roughly the same energy ordering of the d-based MOs, namely, $a_{1-2} (d_\sigma) \leq a_2 (d_\delta) \leq a_{1-1} (d_\sigma) < b_2 (d_\pi) < b_1 (d_\pi)$ (the orbitals being listed from low to high orbital energy). The qualitative shapes of these MOs are similar across all the compounds studied and are depicted in Figure 3 for (nacnac)Ni^{III}(NPh). Actually, all the compounds examined in this study, including the oxo species, exhibit essentially the same energy ordering of the d-type MOs. This strongly suggests that this orbital ordering (though not the exact energy spacing) is largely determined by the C_{2v} -type trigonal-planar geometry of these complexes, rather than by just the imido ligand.

The various metal–NPh (as well as NMe) complexes studied exhibit the following electronic configurations:

$$(\text{nacnac})\text{Cr}^{\text{III}}(\text{NPh}), S = 3/2: d_{y^2}^1 d_{x^2-z^2}^1 d_{xy}^1 d_{xz}^0 d_{yz}^0$$

$$(\text{nacnac})\text{Mn}^{\text{III}}(\text{NPh}), S = 2: d_{y^2}^1 d_{x^2-z^2}^1 d_{xy}^1 d_{xz}^0 d_{yz}^1$$

$$(\text{nacnac})\text{Fe}^{\text{III}}(\text{NPh}), S = 3/2: d_{y^2}^1 d_{x^2-z^2}^1 d_{xy}^2 d_{xz}^0 d_{yz}^1$$

$$(\text{nacnac})\text{Fe}^{\text{IV}}(\text{NPh}), S = 1: d_{y^2}^1 d_{x^2-z^2}^1 d_{xy}^2 d_{xz}^0 d_{yz}^0$$

$$(\text{nacnac})\text{Co}^{\text{III}}(\text{NPh}), S = 0: d_{y^2}^2 d_{x^2-z^2}^2 d_{xy}^2 d_{xz}^0 d_{yz}^0$$

$$(\text{nacnac})\text{Ni}^{\text{III}}(\text{NPh}), S = 1/2: d_{y^2}^2 d_{x^2-z^2}^2 d_{xy}^2 d_{xz}^0 d_{yz}^1$$

$$(\text{nacnac})\text{Cu}^{\text{III}}(\text{NPh}), S = 1: d_{y^2}^2 d_{x^2-z^2}^2 d_{xy}^2 d_{xz}^1 d_{yz}^1$$

The finding that the orbital ordering in these imido complexes (see Figure 2) is rather similar to that in a much weaker-field complex such as (nacnac)NiCl (Figure 1) is quite remarkable and has not been adequately emphasized in the literature. A key point here is that the d_σ -type a_{1-2} MO, which has a lobe pointing directly at the imido nitrogen, has a much lower orbital energy than either of the two d_π -type MOs. This is understandable in the case of a chloride complex such as (nacnac)NiCl but calls for a closer examination for the imido complexes, in view of the much stronger ligand field strength of imido ligands.

The shape of the a_{1-2} MO, the HOMO-4 in Figure 3, provides a clue to its stability. Its d character is best described as $d_{x^2-z^2}$, z being the direction of the metal–imido axis. Although the $d_{x^2-z^2}$ orbital suffers a head-on antibonding interaction with the imido σ lone pair, the repulsion is less than it would be with a d_z^2 orbital, which would stick out further in the z direction. Second, as shown in Figure 3, the lateral lobes of the $d_{x^2-z^2}$ orbital actually engage in a bonding interaction with the imido group. Third, as shown in Table 1, small amounts of Fe s and p character also play a role in muting the Fe(d_σ)–N(p_σ) antibonding interaction. We propose that it is this unusual orbital topology, resulting from the absence of both equatorial and trans ligands, relative to the imido group, that effectively quenches the σ -antibonding nature of this MO.

Two further points are worth making in this connection. First, the topology of the above-mentioned orbital is somewhat different from that of the d_z^2 -based MO that is also unusually stable and occupied in pseudotetrahedral Fe(III) and Co(III) imido complexes.⁵ In this case, much larger admixtures of p_z character appear to be a key factor that minimizes the metal–ligand antibonding interaction. While details of these calculations have been described elsewhere, Figure 4 presents key DFT results for Fe^{III}(MeBP₃)(NMe) (MeBP₃ is a monoanionic methytrisphosphinoborate model ligand),^{42,43} a model pseudotetrahedral imido complex, including a graphical representation of the d_z^2 -based singly occupied molecular orbital (SOMO). Second, we are aware of another example, $S = 1/2$ Fe(5,5-tropocoronand)(NO), from the nitrosyl literature,⁴⁴ where the muted antibonding interaction between a relatively stereochemically inactive Fe $d_{x^2-z^2}$ orbital and the NO lone pair in the singly occupied

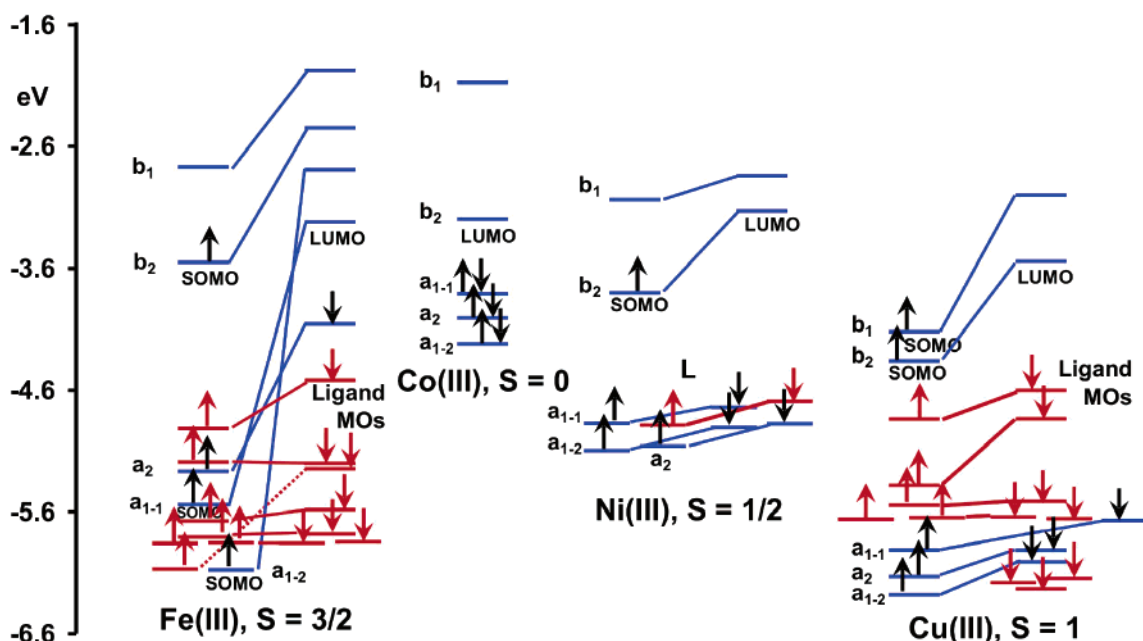


Figure 2. MO energy level diagrams for (nacnac) $M^{III}(\text{NPh})$, $M = \text{Fe, Co, Ni, and Cu}$. Primarily metal-based MOs are indicated in blue and primarily ligand-based MOs in red.

Table 1. Atomic Contributions of the Primarily 3d-Based Majority-Spin MOs for (nacnac) $M^{III}(\text{NPh})$; $M = \text{Fe, Co, Ni, and Cu}$ ^a

metal	S	a_{1-2}	a_2	a_{1-1}	b_2	b_1
Fe(III)	3/2	HOMO-10, (SOMO): 78% Fe (70% $d_{x^2-y^2}$, 5% d_{z^2} , 3% s)	HOMO-3: 83% Fe (d_{xy})	HOMO-4, (SOMO): 62% Fe (50% d_{z^2} , 2% p, 10% s), 9% N_{imido}	HOMO (SOMO): 19% Fe (d_{yz}), 31% N_{imido}	LUMO: 36% Fe (d_{xz}), 38% N_{imido}
Co(III)	0	HOMO-2: 83% Co (63% d_{z^2} , 6% $d_{x^2-y^2}$, 2% p, 12% s), 7% N_{imido}	HOMO-1: 84% Co (d_{xy})	HOMO: 93% Co (86% $d_{x^2-y^2}$, 5% d_{z^2} , 2% p)	LUMO: 40% Co (d_{yz}), 20% N_{imido}	LUMO+1: 43% Co (d_{xz}), 23% N_{imido}
Ni(III)	1/2	HOMO-4: 81% Ni (39% d_{z^2} , 37% $d_{x^2-y^2}$, 3% p, 2% s), 6% N_{imido}	HOMO-3: 86% Ni (d_{xy})	HOMO-1: 92% Ni (54% $d_{x^2-y^2}$, 28% d_{z^2} , 10% s)	HOMO (SOMO): 24% Ni (d_{yz}), 26% N_{imido}	LUMO: 40% Ni (d_{xz}), 30% N_{imido}
Cu(III)	1	HOMO-9: 88% Cu (71% $d_{x^2-y^2}$, 14% d_{z^2} , 3% s)	HOMO-8: 64% Cu (d_{xy})	HOMO-7: 82% Cu (60% d_{z^2} , 16% $d_{x^2-y^2}$, 4% p, 2% s) 6% N_{imido}	HOMO-1 (SOMO): 11% Cu (d_{yz}), 19% N_{imido}	HOMO (SOMO): 32% Cu (d_{xz}), 26% N_{imido}

^a This table accompanies Figure 2.

MO results in a linear NO ligand,^{45,46} which is very uncommon for low-spin $\{\text{FeNO}\}^7$ complexes.⁴⁷ It is thus becoming clear that an increasing number of novel structural and stereochemical phenomena may be attributed to specific d-orbital hybridizations resulting from low-coordinate environments, as opposed to “normal” octahedral ones.

The MO topologies and symmetries, as presented above, allow an appreciation of the variations in the metal– N_{imido} distances and molecular spin-density profiles for the various first-row transition-metal complexes, as discussed in the next two sections.

B. Structural Chemistry. Selected optimized geometry parameters and Mulliken spin populations for NMe, NPh, and oxo complexes are listed in Tables 2 and 3, respectively.

Much of the same information is depicted graphically for NMe and NPh complexes in Figures 5 and 6, respectively. Let us first discuss trends in the metal–imido distance among the middle transition metals (Cr, Mn, and Fe). From $S = 3/2$ Cr(III) to $S = 2$ Mn(III), the metal– N_{imido} distance expands slightly, by a couple of hundredths of an angstrom, reflecting the single d_{π} – p_{π} antibonding interaction in the Mn(III) complexes. The effect is slight because it is superimposed on the tendency of ionic radii to shrink from left to right across a transition series, because of less effective shielding of the inner electrons. Thus, from $S = 2$ Mn(III) to $S = 3/2$ Fe(III), the metal–imido distance shrinks by about 0.03 Å, although both ions feature a single d_{π} – p_{π} antibonding interaction in their respective complexes. The metal– N_{imido}

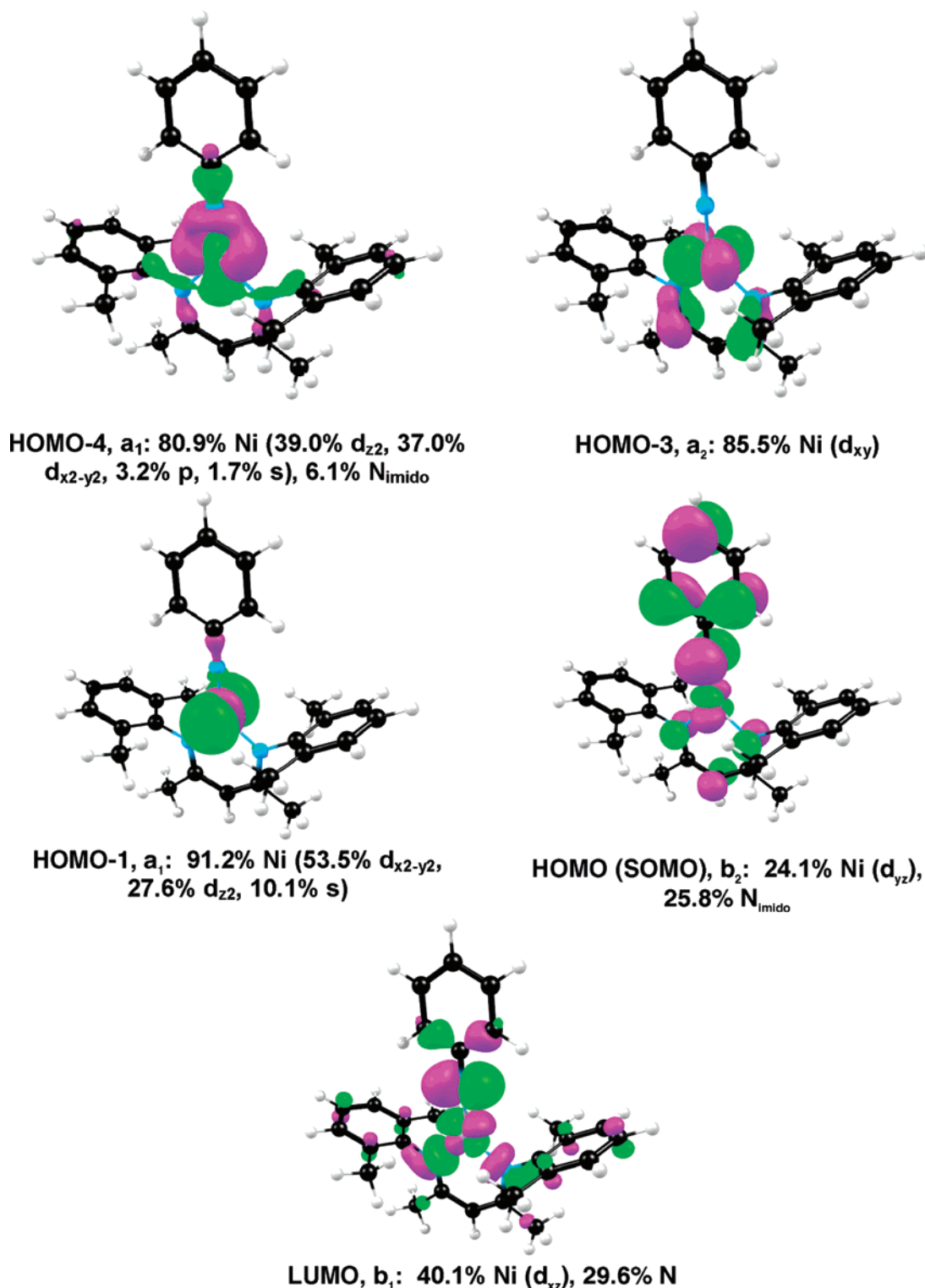


Figure 3. Plots of the primarily 3d-based majority-spin MOs of (nacnac) $N^{\text{III}}(\text{NPh})$.

distances in the three different spin states of the Fe(III) complexes nicely illustrate the effect of the number of the number π -antibonding interactions. Thus, from low-spin to intermediate-spin Fe(III), the Fe– N_{imido} distance increases by about 0.03 Å, while going to high-spin Fe(III) increases this distance by at least another 0.05 Å. Unfortunately, no middle transition-metal nacnac imido complex has been isolated and structurally characterized, so these structural trends appear to be largely of predictive value. Holland and

co-workers, however, apparently have generated a three-coordinate $S = 3/2$ Fe(III)–imido complex in solution; however, no experimental metrical parameters are as yet available for this species.^{19,48}

Our optimized Co and Ni imido structures are in excellent agreement with the crystallographic structures of very similar compounds.^{20,21} Thus, the PW91 (1.625 Å) and OLYP (1.627 Å) Co–NMe distances agree well with the Co–NAd (1.624 Å) distance in the experimentally studied cobalt complex.²⁰

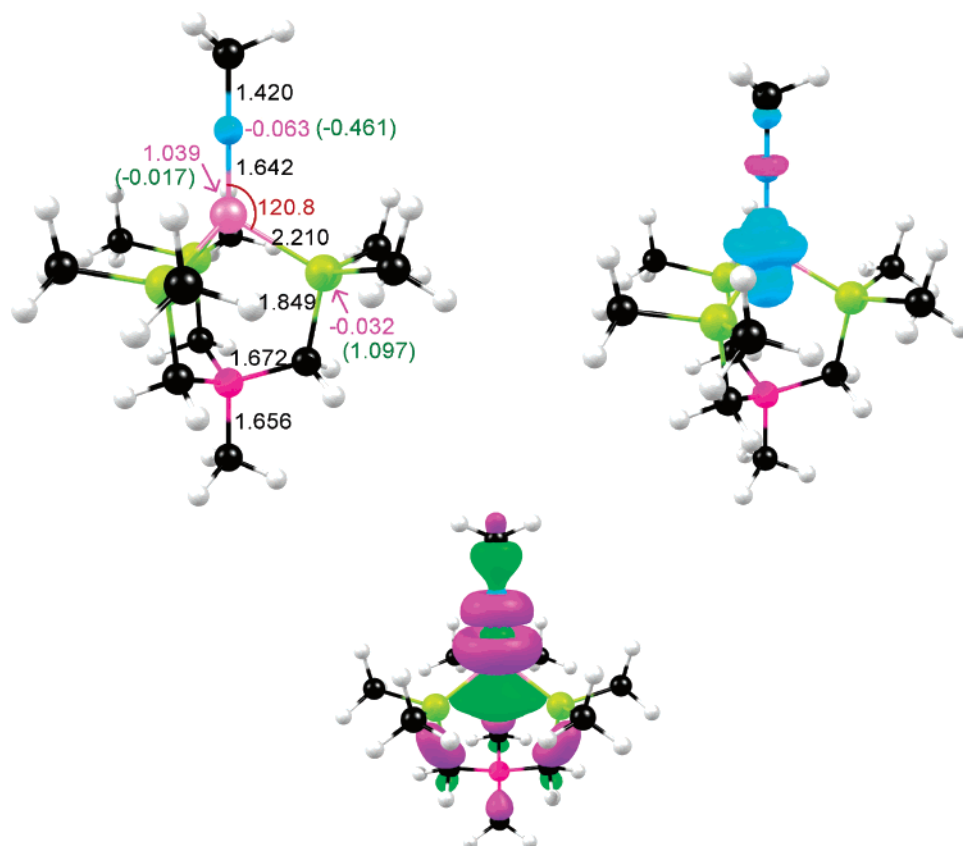


Figure 4. Selected results for $\text{Fe}^{\text{III}}(\text{MeBP}_3)(\text{NMe})$ (C_{3v}), a pseudotetrahedral Fe(III) imido complex. Top left: Optimized distances (Å, in black), angles (deg, red), Mulliken spin populations (magenta), and charges (green, in parentheses). Top right: A plot of the spin density, with majority and minority spin densities indicated in cyan and magenta, respectively. Bottom: A plot of the SOMO.

Likewise, the PW91 (1.668 Å) and OLYP (1.675 Å) Ni–NMe distances agree well with an experimental Ni–NAD distance of 1.662 Å.²¹ Note that the optimized Cu–NMe distances (PW91 1.762 Å and OLYP 1.782 Å) are longer still. The increase in the metal– N_{imido} distance from Co(III) to Ni(III) to Cu(III) nicely reflects the increasing number of d_{π} – p_{π} antibonding interactions along the series of metal ions – 0, 1, and 2, respectively.

C. Spin-Density Profiles. Figures 5 and 6 present graphical representations of the spin-density profiles of key NMe and NPh complexes, while Tables 2 and 3 present listings of Mulliken spin populations. The MO descriptions of the complexes given above allow us to readily appreciate the spin-density profiles, as discussed case by case below.

Cr(III). The $d_{yz}^1 d_{xz}^2 - z^1 d_{xy}^1$ electronic configuration suggests that most of the excess spin density should be localized on the metal. This is indeed the case; however, both PW91 and OLYP calculations indicate a substantial minority spin density on the imido nitrogen. Careful examination of the shapes of the different valence MOs indicates that this excess minority spin density results from a slight spatial offset between the α - and β -spin forms of the d_{π} – p_{π} bonding MOs. Such spatially offset π bonding is actually relatively common in open-shell transition-metal complexes, and we have seen a similar occurrence in a NO complex, $\text{Mo}(\text{P})(\text{NO})(\text{MeOH})$ (P = porphyrin), which has a $\{\text{MoNO}\}^5 d_{\pi}^2 d_{\pi'}^2 d_{\sigma}^1$ configuration but, nonetheless, exhibits a significant amount of minority spin density on the NO.⁴⁹

Mn(III) and Fe(III). In these cases, note from Figures 5 and 6 that the spin-density profile is highly anisotropic at the imido nitrogen. While a dumbbell of majority spin density reflects single occupancy of the d_{yz} -based b_2 MO, note the dumbbell of minority spin density in the xz plane (once again, reflecting a spatially offset π bonding in the xz plane). As a result, there is only a tiny amount of excess spin density on the imido nitrogens of these complexes.

Fe(IV). Crudely speaking, the spin-density profile of the cationic $S = 1$ Fe(IV) complexes resembles those of the Cr(III) complexes, as expected from the $d_{yz}^1 d_{xz}^2 - z^1 d_{xy}^2$ electronic configuration of the former. As in the Cr(III) case, a cylindrically symmetric blob of minority spin density resides on the imido nitrogen.

We will not have much occasion to discuss the Mulliken charges shown in Figures 5 and 6. However, note that the Fe, N_{imido} , and N_{nacnac} charges are only slightly higher in the cationic Fe(IV) case than in the Fe(III) case, consistent with the electroneutrality principle.

Ni(III). The $S = 1/2$ Ni(III) spin density mirrors the form of the singly occupied b_2 d_{π} -based orbital. Note that the spin density partitions itself roughly 1:2 between the Ni and the N_{imido} . In other words, as previously noted,²¹ the Ni(III) complexes may be described as having substantial $\text{Ni}^{\text{II}}\text{--NR}^{\text{+}}$ character.

Cu(III). The cylindrically symmetric $S = 1$ Cu(III) spin density corresponds faithfully to a pair of singly occupied d_{π} -based orbitals. In this case, the spin density is even more

Table 2. Selected Geometry Parameters (Å, deg) and Mulliken Spin Populations for (nacnac)M(NMe) Complexes Optimized under a C_s Symmetry Constraint

metal ion	charge	S	M–N _{imido}		M–N _{nacnac} ^a		∠(NMN) _{nacnac}	
			PW91	OLYP	PW91	OLYP	PW91	OLYP
Cr(III)	0	3/2	1.686	<i>b</i>	2.016	<i>b</i>	131.5	<i>b</i>
Mn(III)	0	1	1.660	<i>b</i>	1.909	<i>b</i>	130.3	<i>b</i>
Mn(III)	0	2	1.703	1.723	2.010	2.041	131.6	131.2
Fe(III)	0	1/2	1.633	1.639	1.891	1.911	131.4	129.9
Fe(III)	0	3/2	1.673	1.686	1.958	1.955	128.6	129.9
Fe(III)	0	5/2	1.749	1.750	2.016	2.058	109.0	111.8
Fe(IV)	1	1	1.657	1.658	1.881	1.920	129.8	132.4
Fe(IV)	1	2	1.690	1.693	1.913	1.943	108.7	113.7
Co(III)	0	0	1.625	1.627	1.856	1.876	132.3	132.5
Co(III)	0	1	1.666	1.683	1.911	1.943	129.0	131.6
Co(III)	0	2	1.747	1.751	1.965	1.998	111.5	112.7
Ni(III)	0	1/2	1.668	1.675	1.883	1.910	130.9	130.8
Ni(III)	0	3/2	1.745	1.753	1.924	1.956	107.9	109.8
Cu(III)	0	0	1.723	1.738	1.926	1.960	130.5	130.9
Cu(III)	0	1	1.762	1.782	1.951	1.990	130.4	130.4

metal ion	charge	S	S _M		S _{N(imido)}		S _{N(nacnac)} ^a	
			PW91	OLYP	PW91	OLYP	PW91	OLYP
Cr(III)	0	3/2	3.359	<i>b</i>	−0.458	<i>b</i>	−0.065	<i>b</i>
Mn(III)	0	1	2.533	<i>b</i>	−0.335	<i>b</i>	−0.045	<i>b</i>
Mn(III)	0	2	4.018	4.174	−0.067	−0.210	−0.042	−0.037
Fe(III)	0	1/2	1.376	1.550	−0.289	−0.419	−0.017	−0.017
Fe(III)	0	3/2	2.769	2.949	0.135	0.067	−0.025	−0.001
Fe(III)	0	5/2	3.747	3.744	0.964	0.975	0.036	0.037
Fe(IV)	1	1	2.325	2.533	−0.275	−0.499	−0.036	−0.049
Fe(IV)	1	2	3.042	3.266	0.587	0.425	0.057	0.058
Co(III)	0	0						
Co(III)	0	1	1.655	1.648	0.281	0.307	0.016	0.016
Co(III)	0	2	2.543	2.540	1.114	1.141	0.071	0.073
Ni(III)	0	1/2	0.332	0.303	0.598	0.652	0.014	0.005
Ni(III)	0	3/2	1.272	1.287	1.270	1.293	0.105	0.101
Cu(III)	0	0						
Cu(III)	0	1	0.330	0.331	1.361	1.404	0.068	0.063

^a Average bond distance ^b SCF cycles did not converge.

polarized toward the imido nitrogen, split 1:5, in fact, between the Cu and N_{imido}. Thus, once again, we have a highly noninnocent imido ligand, and the complex might well be described as a Cu(I) triplet-nitrene conglomerate.

A comment is in order on the small differences in spin-density profile between the NMe and NPh complexes. The difference is especially pronounced when the *b*₂ d_π-based MO is singly occupied, as in the Ni(III) case. In this case, both the Ni and the imido nitrogens in the NPh complexes carry a smaller amount of spin density, relative to their NMe analogues; the difference is accounted for by the presence of some spin density at the ortho and para carbons of the NPh group.

D. Spin-State Energetics and the Performance of Different Functionals. We now come to what we view as the heart of this study. The energetics of the low-lying spin states of transition-metal complexes is not only a core issue for coordination chemistry but also an important one for computational studies. In particular, this is still a problematic issue for DFT calculations. Classic “pure” functionals such as PW91 typically unduly favor states with lower spin

Table 3. Selected Geometry Parameters (Å, deg) and Mulliken Spin Populations for (nacnac)M(NPh) Complexes Optimized under a C_{2v} Symmetry Constraint

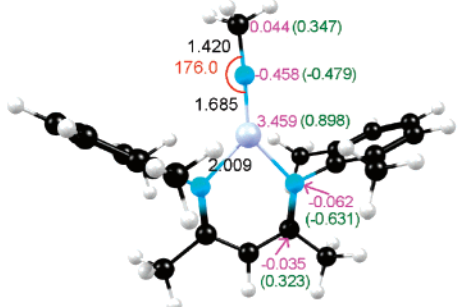
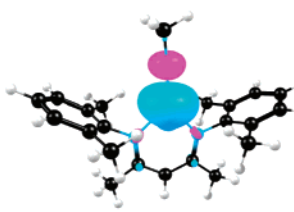
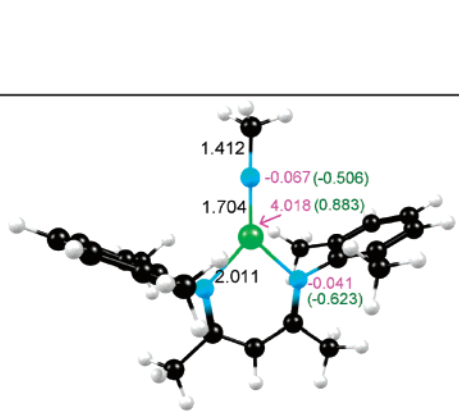
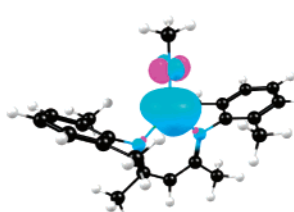
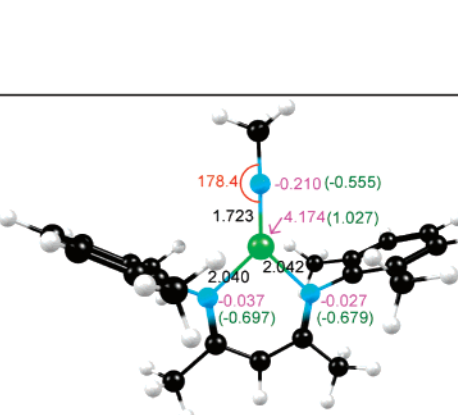
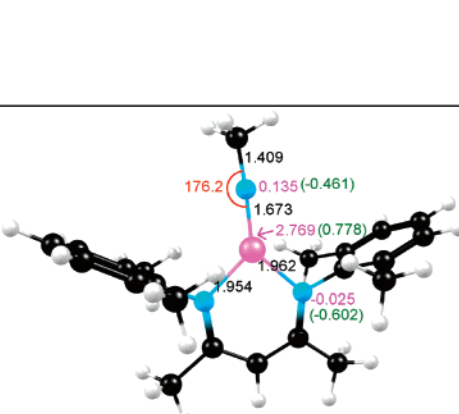
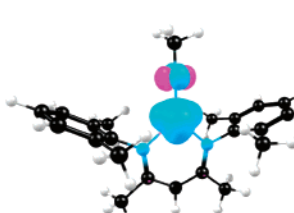
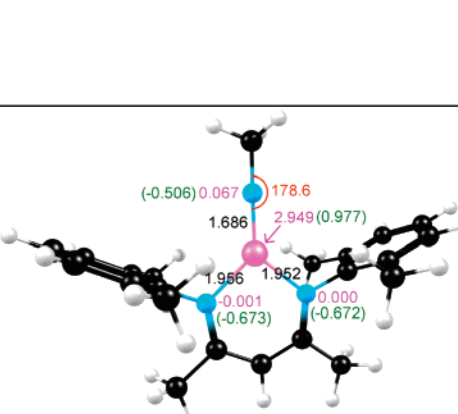
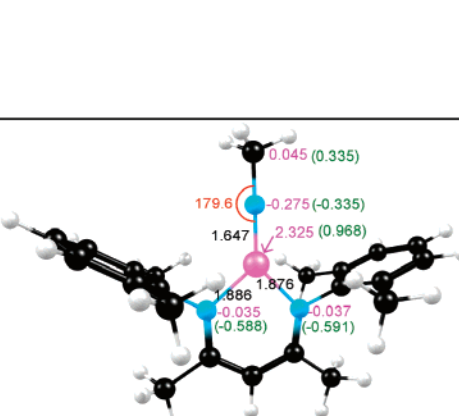

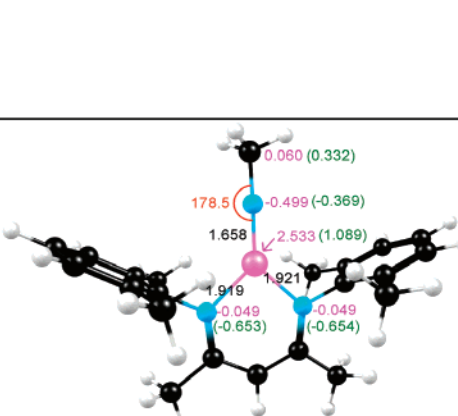
metal ion	charge	S	M–N _{imido}		M–N _{nacnac}		∠(NMN) _{nacnac}	
			PW91	OLYP	PW91	OLYP	PW91	OLYP
Cr(III)	0	3/2	1.710	1.712	2.010	2.004	134.7	133.6
Mn(III)	0	1	1.685	<i>a</i>	1.905	<i>a</i>	133.1	<i>a</i>
Mn(III)	0	2	1.716	1.736	1.995	2.028	133.0	132.3
Fe(III)	0	1/2	1.658	1.671	1.887	1.913	1.333.0	132.5
Fe(III)	0	3/2	1.688	1.700	1.912	1.947	131.8	131.4
Fe(III)	0	5/2	1.753	1.756	2.016	2.064	130.9	131.1
Fe(IV)	1	1	1.674	1.692	1.883	1.907	133.1	132.4
Fe(IV)	1	2	1.712	1.722	1.907	1.936	129.6	129.2
Co(III)	0	0	1.647	1.653	1.852	1.872	133.4	133.2
Co(III)	0	1	1.691	1.700	1.909	1.932	132.9	133.0
Co(III)	0	2	1.743	1.746	1.973	2.018	130.0	130.4
Ni(III)	0	1/2	1.682	1.690	1.875	1.903	132.5	132.5
Ni(III)	0	3/2	1.732	1.743	1.923	1.959	126.7	126.4
Cu(III)	0	0	1.758	1.774	1.940	1.972	131.7	131.7
Cu(III)	0	1	1.769	1.789	1.948	1.985	131.5	131.5

metal ion	charge	S	S _M		S _{N(imido)}		S _{N(nacnac)}	
			PW91	OLYP	PW91	OLYP	PW91	OLYP
Cr(III)	0	3/2	3.517	3.511	−0.414	−0.412	−0.070	−0.070
Mn(III)	0	1	2.600	<i>a</i>	−0.302	<i>a</i>	−0.047	<i>a</i>
Mn(III)	0	2	3.946	4.112	−0.134	−0.280	−0.042	−0.035
Fe(III)	0	1/2	1.450	1.647	−0.273	−0.396	−0.019	−0.020
Fe(III)	0	3/2	2.739	2.873	0.075	−0.034	−0.003	0.002
Fe(III)	0	5/2	3.801	3.786	0.755	0.788	0.015	0.021
Fe(IV)	1	1	2.406	2.617	−0.243	−0.372	−0.018	−0.009
Fe(IV)	1	2	3.314	3.410	0.177	0.106	0.011	0.017
Co(III)	0	0						
Co(III)	0	1	1.556	1.549	0.165	0.164	0.014	0.016
Co(III)	0	2	2.602	2.589	0.895	0.926	0.052	0.053
Ni(III)	0	1/2	0.276	0.263	0.381	0.414	0.017	0.011
Ni(III)	0	3/2	1.378	1.378	1.049	1.078	0.077	0.073
Cu(III)	0	0						
Cu(III)	0	1	0.324	0.304	1.058	1.099	0.072	0.068

^a SCF cycles did not converge.

multiplicities, while hybrid functionals have been documented to behave oppositely. In this study, we have carried out single-point energy calculations on the OLYP optimized geometries of all the NPh and oxo complexes studied. These results afford a wealth of information on (a) trends in spin-state energetics in nacnac imido complexes, (b) the performance of the different functionals, and (c) comparisons of NPh and oxo spin-state energetics. The various energetics results are shown in Tables 5–7. All of these issues are discussed below on a case by case basis.

Mn(III). For Mn(III) imido complexes, the “pure” functionals such as PW91, BLYP, BP, and XLYP indicate nearly isoenergetic *S* = 1 and 2 states. In contrast, the newer “pure” functionals OLYP and OPBE, which include the Handy–Cohen exchange OPTX exchange functional, favor the *S* = 2 state by about 0.7 and 0.5 eV, respectively. The three hybrid functionals examined also favor the *S* = 2 state by a similar margin. The *S* = 0 state is far higher in energy than either the *S* = 1 or 2 state. Overall, the results suggest an *S* = 2 ground state.

PW91		OLYP
 <p>1.420 176.0 1.685 2.009 0.044 (0.347) -0.458 (-0.479) 3.459 (0.898) -0.062 (-0.631) -0.035 (0.323)</p>		
(nacnac)Cr ^{III} (NMe), S = 3/2		
 <p>1.412 1.704 2.011 -0.067 (-0.506) 4.018 (0.883) -0.041 (-0.623)</p>		 <p>178.4 1.723 2.040 2.042 -0.210 (-0.555) 4.174 (1.027) -0.037 (-0.697) -0.027 (-0.679)</p>
(nacnac)Mn ^{III} (NMe), S = 2		
 <p>1.409 176.2 1.673 1.962 1.954 -0.135 (-0.461) 2.769 (0.778) -0.025 (-0.602)</p>		 <p>(-0.506) 0.067 178.6 1.686 1.956 1.952 2.949 (0.977) -0.001 (-0.673) 0.000 (-0.672)</p>
(nacnac)Fe ^{III} (NMe), S = 3/2		
 <p>0.045 (0.335) 179.6 1.647 1.886 1.876 -0.275 (-0.335) 2.325 (0.968) -0.035 (-0.588) -0.037 (-0.591)</p>		 <p>0.060 (0.332) 178.5 1.658 1.919 1.921 -0.499 (-0.369) 2.533 (1.089) -0.049 (-0.653) -0.049 (-0.654)</p>
[(nacnac)Fe ^{IV} (NMe)] ⁺ , S = 1		

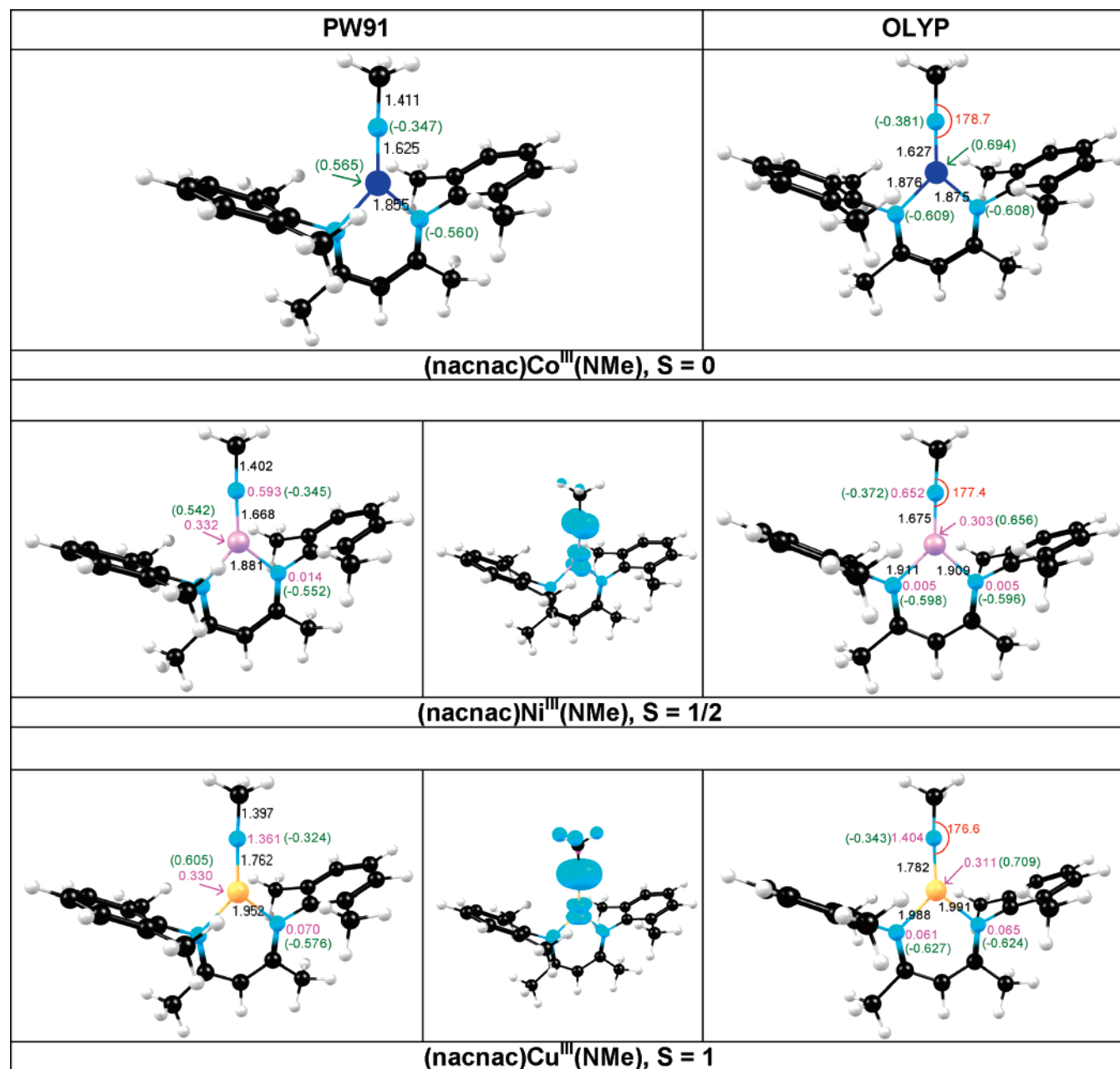


Figure 5. Calculated results for (nacnac)M(NMe) complexes for M = Cr^{III} (S = 3/2), Mn^{III} (S = 2), Fe^{III} (S = 3/2), Fe^{IV} (S = 1), Co (S = 0), Ni (S = 1/2), and Cu (S = 1): PW91- and OLYP-optimized distances (Å, black), Mulliken charges (green), and spin populations (magenta); for the open-shell species, PW91 spin-density plots are also shown, with majority and minority spin densities in cyan and magenta, respectively. Color code for atoms: C (black), H (white), N (magenta), Cr (light blue), Mn (green), Fe (cyan), Co (royal blue), Ni (pink), and Cu (light orange).

Fe(III). For (nacnac)Fe^{III}(NMe), as shown in Table 5, the “classic” PW91 functional predicts an S = 1/2 ground state by a clear margin of energy, in apparent disagreement with an electron paramagnetic resonance and Mössbauer analysis on a closely related species, while the newer Handy–Cohen OLYP functional predicts an S = 3/2 ground state, by a clear margin of energy, apparently consistent with experimental results. For (nacnac)Fe^{III}(NPh), as shown in Tables 5 and 6, the pure functionals such as PW91, BLYP, BP, and XLYP indicate nearly isoenergetic S = 1/2 and 3/2 states and an S = 5/2 state nearly 0.9 eV higher in energy.^{50,51} The OLYP and OPBE functionals predict S = 3/2 ground states, S = 1/2 excited states 0.3–0.4 higher in energy, and S = 5/2 excited states about 0.5 eV higher in energy than the ground states.

In contrast, the hybrid functionals do predict S = 3/2 ground states but switch the ordering of the S = 1/2 and 5/2 states, relative to OLYP and OPBE.

Co(III). For Co(III) imido complexes, all the pure functionals examined clearly predict an S = 0 ground state, consistent with experimental results, while the hybrid functionals predict higher-multiplicity spin states. Thus, at least for the spin-state energetics of the Co(III) imido complexes, the pure functionals appear to be significantly better. Note once again that the newer pure functionals OLYP and OPBE behave somewhat differently from the older ones; thus, the older pure functionals predict substantially higher relative energies for the S = 2 state, compared with OLYP and OPBE.

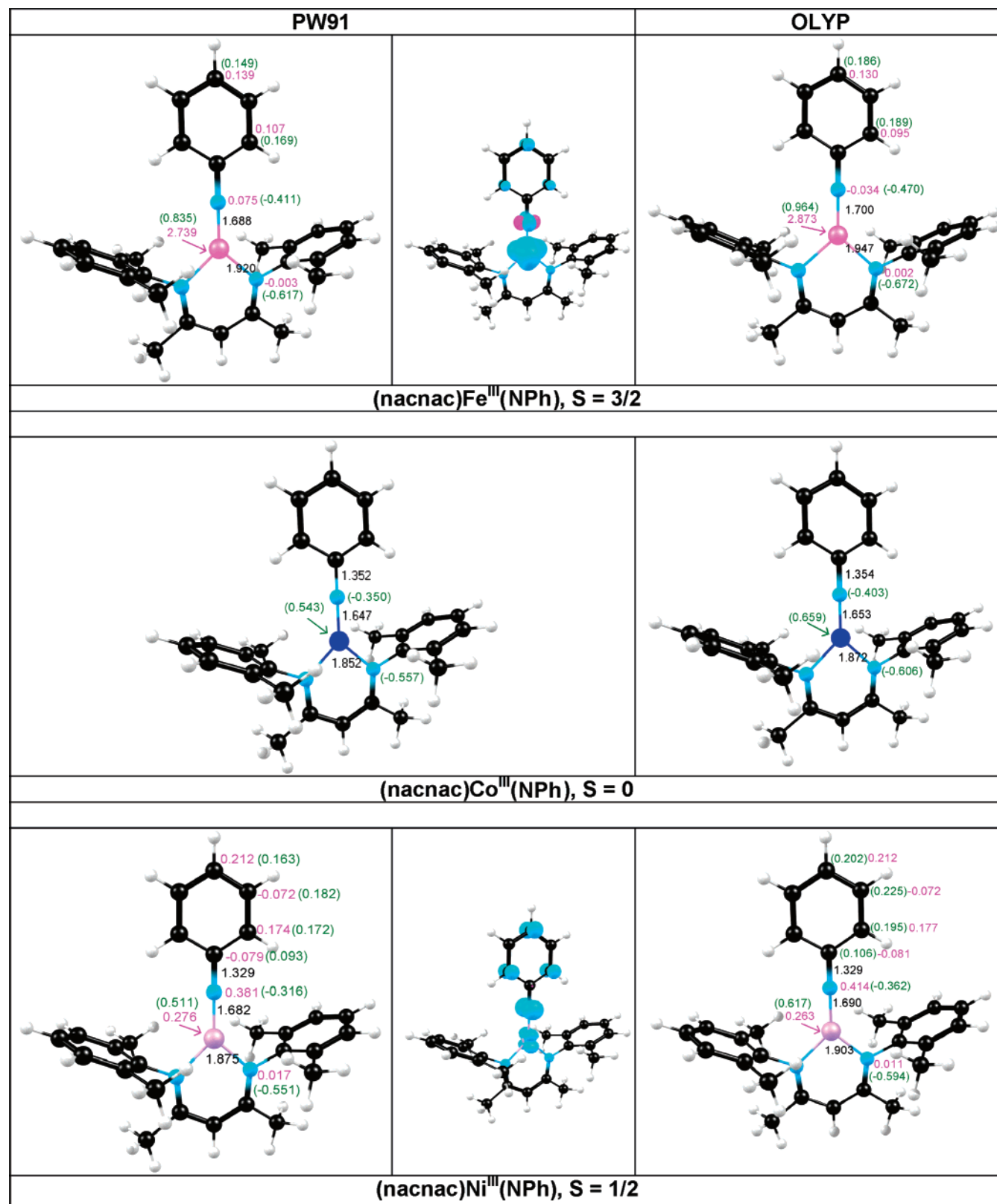


Figure 6. Calculated results for selected (nacnac)M(NPh) complexes for M = Fe^{III} (S = 3/2), Co (S = 0), and Ni (S = 1/2): PW91- and OLYP-optimized distances (Å, black), Mulliken charges (green), and spin populations (magenta); for the open-shell species, PW91 spin-density plots are also shown, with majority and minority spin densities in cyan and magenta, respectively. Color code for atoms: same as in Figure 5.

Ni(III) and Cu(III). All the functionals examined, whether pure or hybrid, predict S = 1/2 and S = 1 ground states for the Ni(III) and Cu(III) complexes, respectively, by a clear margin of energy.

The above results afford remarkable insights into the relative performance of the different functionals. In the case of the Fe(III) imido complexes, the classic pure functionals fail to predict an S = 3/2 ground state, as observed

Table 4. Selected Geometry Parameters (Å, deg) and Mulliken Spin Populations for (nacnac)M(O) Complexes Optimized under C_{2v} Symmetry Constraints

metal ion	charge	S	M–O		M–N _{nacnac}		$\angle(\text{NMN})_{\text{nacnac}}$	
			PW91	OLYP	PW91	OLYP	PW91	OLYP
Cr(III)	0	$3/2$	1.641	<i>a</i>	1.997	<i>a</i>	135.5	<i>a</i>
Mn(III)	0	1	1.619	1.623	1.984	1.907	133.7	132.9
Mn(III)	0	2	1.659	1.668	1.984	2.009	133.5	132.5
Fe(III)	0	$1/2$	1.600	1.599	1.844	1.854	132.5	131.9
Fe(III)	0	$3/2$	1.634	1.639	1.909	1.917	132.1	131.0
Fe(III)	0	$5/2$	1.682	1.684	2.013	2.038	131.3	130.6
Fe(IV)	1	1	1.610	1.612	1.865	1.880	133.4	132.1
Fe(IV)	1	2	1.647	1.648	1.888	1.914	130.0	129.0
Co(III)	0	0	1.633	1.637	1.842	1.855	134.2	133.6
Co(III)	0	1	1.616	1.616	1.858	1.880	131.8	131.4
Co(III)	0	2	1.666	1.666	1.963	2.002	130.6	130.6
Ni(III)	0	$1/2$	1.667	1.675	1.872	1.894	133.3	133.1
Ni(III)	0	$3/2$	1.654	1.655	1.924	1.962	130.0	130.1
Cu(III)	0	0	1.718	1.727	1.934	1.967	132.9	132.6
Cu(III)	0	1	1.735	1.748	1.948	1.986	132.9	132.4

metal ion	charge	S	S _M		S _O		S _{N(nacnac)}	
			PW91	OLYP	PW91	OLYP	PW91	OLYP
Cr(III)	0	$3/2$	3.185	<i>a</i>	−0.170	<i>a</i>	−0.080	<i>a</i>
Mn(III)	0	1	2.202	2.382	−0.005	−0.090	−0.061	−0.073
Mn(III)	0	2	3.822	3.938	0.166	0.076	−0.051	−0.050
Fe(III)	0	$1/2$	0.946	1.029	0.148	0.126	−0.026	−0.037
Fe(III)	0	$3/2$	2.638	2.728	0.404	0.363	−0.010	−0.013
Fe(III)	0	$5/2$	3.913	3.909	0.872	0.893	0.037	0.038
Fe(IV)	1	1	2.161	2.333	0.195	0.181	−0.122	−0.154
Fe(IV)	1	2	3.250	3.373	0.595	0.629	0.024	0.009
Co(III)	0	0						
Co(III)	0	1	1.386	1.412	0.621	0.626	0.015	0.004
Co(III)	0	2	2.707	2.705	1.032	1.053	0.090	0.088
Ni(III)	0	$1/2$	0.409	0.384	0.551	0.618	0.024	0.013
Ni(III)	0	$3/2$	1.478	1.485	1.159	1.179	0.131	0.124
Cu(III)	0	0						
Cu(III)	0	1	0.457	0.425	1.140	1.190	0.139	0.133

^a SCF cycles did not converge.

experimentally, unduly favoring an $S = 1/2$ state instead. In the case of the Co(III) imido complexes, the hybrid functionals fail to yield $S = 0$ ground states, as observed experimentally. That leaves only the newer pure functionals OLYP and OPBE, which yield energetics that, as far as we know, are entirely consistent with experimental results in this field.

In turn, these raise the prospect of a tantalizing scenario. If the OLYP (and OPBE) energetics are really semiquantitatively accurate—and there is a certain leap of faith here—then the OLYP/OPBE columns in Tables 5–7 offer for the first time a good *global* picture of the spin-state energetics of the many different nacnac imido and oxo species studied. Whether or not this is actually the case will become clearer as more experimental data accumulate.

E. Spin-State Energetics of the Oxo Species. We have mentioned above that imido and oxo species exhibit roughly the same orbital energy ordering. However, the orbital energy spacings are significantly different, leading, in a few cases, to different spin-state energetics (Table 7), relative to the imido complexes (Table 6). Some highlights of our results

Table 5. PW91 and OLYP Energies (eV) for Different Spin States of NMe, NPh, and Oxo Complexes^a

metal	S	axial ligand					
		NMe		NPh		oxo	
		PW91	OLYP	PW91	OLYP	PW91	OLYP
Mn(III)	2	0.00	0.00	0.00	0.00	0.00	0.00
	1	−0.02	0.52	0.11	0.73	0.20	0.53
	0	2.49	2.68	1.28	2.92	0.54	0.87
Fe(III)	$3/2$	0.00	0.00	0.00	0.00	0.00	0.00
	$5/2$	0.53	0.46	0.91	0.53	0.78	0.36
	$1/2$	−0.36	0.16	0.00	0.29	0.44	0.73
Fe(IV)	1	0.00	0.00	0.00	0.00	0.00	0.00
	2	0.55	0.25	0.86	0.62	0.43	0.14
Co(III)	0	0.00	0.00	0.00	0.00	0.00	0.00
	1	0.47	0.33	0.37	0.20	−0.36	−0.56
Ni(III)	2	0.90	0.45	1.02	0.53	0.07	−0.48
	$1/2$	0.00	0.00	0.00	0.00	0.00	0.00
Cu(III)	$3/2$	0.67	0.47	1.16	0.88	0.26	−0.06
	1	0.00	0.00	0.00	0.00	0.00	0.00
Cu(III)	0	0.45	0.57	1.28	1.28	0.40	0.66

^a All energies refer to fully optimized structures, and the energy zero levels are indicated in bold.

are as follows. As in the Fe(III) imido case, the Fe^{III}O complexes also exhibit $S = 3/2$ ground states. However, in contrast to the Co(III) imido case, *all* the functionals examined predict open-shell $S = 1$ or $S = 2$ ground states for the Co^{III}O complexes; thus, while all the pure functionals including OLYP and OPBE favor $S = 1$ ground states, the three hybrid functionals examined favor $S = 2$ ground states. In the Ni^{III}O case, both the newer pure functionals (OLYP and OPBE) and the hybrid functionals favor $S = 3/2$ ground states, while the older pure functionals favor $S = 1/2$ states. In the Cu^{III}O case, all the functionals favor an $S = 1$ state, relative to an $S = 0$ excited state, by several tenths of an electronvolt.

By way of a minor digression, we would like to point out that the calculated spin-state energetics of (nacnac)Cu^{III}O species (which might also be viewed as Cu^{II}–O•) may be relevant for the dioxygen activation mechanisms of “non-coupled” dicopper monooxygenases such as peptidyl α -hydroxylating monooxygenase (PHM) and dopamine β -monooxygenase (DBM).⁵² Although no Cu^{III}O species has been experimentally detected, at least two groups have considered the intermediacy of such species for PHM⁵³ and/or DBM.^{54,55} As in this study, both groups predicted triplet ground states for the Cu^{III}O intermediates considered; however, these studies considered four- and five-coordinate Cu^{III}O species, whereas we have been exclusively concerned with trigonal-planar species in this study.

For the time being, the above results for the oxo species cannot be related to experimental results, but they clearly emphasize that the spin-state energetics of otherwise analogous imido and oxo complexes may be quite different, a prediction we look forward to seeing experimentally confirmed.

F. Adiabatic Electron Affinities. Given that the Ni and Cu complexes studied are high-valent species, we wished to obtain a computational “handle” on their reactivity,

Table 6. Multifunctional Single-Point Energies (eV) of Different Electronic States of NPh Complexes at Optimized OLYP Structures^a

metal	S	BLYP	BP	OPBE	XLYP	B3LYP (VWN5)	O3LYP (VWN5)	X3LYP (VWN5)
Mn(III)	2	0.00	0.00	0.00	0.00	0.00	0.00	0.00
	1	0.08	0.14	0.52	0.09	0.73	0.81	0.78
	0	2.39	2.53	2.99	2.40	3.37	3.43	3.45
Fe(III)	3/2	0.00	0.00	0.00	0.00	0.00	0.00	0.00
	5/2	0.86	0.87	0.53	0.85	0.26	0.23	0.22
	1/2	-0.05	0.01	0.40	-0.05	0.40	0.56	0.43
Co(III)	0	0.00	0.00	0.00	0.00	0.00	0.00	0.00
	1	0.38	0.37	0.18	0.36	-0.25	-0.14	-0.29
	2	0.98	1.01	0.54	0.95	-0.24	-0.12	-0.33
Ni(III)	1/2	0.00	0.00	0.00	0.00	0.00	0.00	0.00
	3/2	1.10	1.14	0.90	1.08	0.55	0.60	0.51
Cu(III)	1	0.00	0.00	0.00	0.00	0.00	0.00	0.00
	0	0.60	0.62	0.68	0.61	0.87	0.88	0.90

^a Energy zero levels are indicated in bold. (This table should be read in conjunction with Table 5.)**Table 7.** Multifunctional Single-Point Energies (eV) of Different Electronic States of Oxo Complexes at Optimized OLYP Structures^a

metal	S	BLYP	BP	OPBE	XLYP	B3LYP (VWN5)	O3LYP (VWN5)	X3LYP (VWN5)
Mn(III)	2	0.00	0.00	0.00	0.00	0.00	0.00	0.00
	1	0.15	0.21	0.58	0.15	0.82	0.90	0.87
	0	0.67	0.79	1.25	0.69	1.78	1.79	1.87
Fe(III)	3/2	0.00	0.00	0.00	0.00	0.00	0.00	0.00
	5/2	0.77	0.75	0.33	0.76	0.16	0.04	0.11
	1/2	0.41	0.45	0.81	0.42	1.09	1.15	1.14
Fe(IV)	1	0.00	0.00	0.00	0.00	0.00	0.00	0.00
	2	0.45	0.42	0.09	0.45	0.08	-0.07	0.05
Co(III)	0	0.00	0.00	0.00	0.00	0.00	0.00	0.00
	1	-0.30	-0.34	-0.62	-0.30	-0.65	-0.78	-0.68
	2	0.08	0.07	-0.52	0.05	-0.97	-1.07	-1.06
Ni(III)	1/2	0.00	0.00	0.00	0.00	0.00	0.00	0.00
	3/2	0.25	0.26	-0.07	0.24	-0.08	-0.24	-0.11
Cu(III)	1	0.00	0.00	0.00	0.00	0.00	0.00	0.00
	0	0.40	0.42	0.58	0.40	0.64	0.70	0.66

^a Energy zero levels are indicated in bold. (This table should be read in conjunction with Table 5.)

especially via reductive pathways. We have done so, admittedly in a crude manner, by calculating the adiabatic electron affinities (EAs) for several of the NPh and oxo complexes studied, which are listed in Table 8. For certain of the complexes, more than one EA has been reported because of multiple contenders for the ground state of either the neutral or anionic species. Our key conclusions vis-à-vis the EAs are as follows.

First, none of the EAs is exceptionally high. Even for (nacnac)Cu^{III}(NPh), the OLYP EA of 1.65 eV is essentially the same as that of the analogous Ni(III) complex. Thus, we speculated that such a Cu(III) imido complex should be experimentally accessible.⁵⁶ Indeed, while this paper was under review, Warren and co-workers reported a transient (nacnac)Cu^I-nitrene intermediate, albeit with no detailed spectroscopic characterization.

Second, compared to imido complexes, the EAs of the oxo complexes are not remarkably high either. Thus, the oxo species appear to be viable as reactive intermediates. However, being sterically unprotected (say, relative to the

Table 8. Adiabatic Electron Affinities (eV) of the (nacnac)M(L) Complexes Studied

	S for neutral	S for anion	EA	
			PW91	OLYP
(nacnac)Fe(NPh)	3/2	1	1.70	1.21
(nacnac)Co(NPh)	0	1/2	1.77	1.52
(nacnac)Ni(NPh)	1/2	0	1.58	1.31
(nacnac)Ni(NPh)	1/2	1	1.52	1.63
(nacnac)Cu(NPh)	1	1/2	1.93	1.65
(nacnac)Fe(O)	3/2	1	1.24	0.77
(nacnac)Co(O)	1	1/2	1.61	1.14
(nacnac)Co(O)	1	3/2	1.62	1.53
(nacnac)Ni(O)	1/2	1	1.43	1.12
(nacnac)Ni(O)	3/2	1	2.09	1.63
(nacnac)Cu(O)	1	1/2	2.11	1.78

adamantylimido complexes studied experimentally), the oxo complexes are likely to be susceptible to dimerization as well as a variety of other reaction pathways.^{20,57}

Third, not surprisingly, the PW91 and OLYP EAs differ significantly in a number of cases. On the basis of our overall findings, we view the OLYP EAs as significantly more accurate.

Conclusion

In summary, we have carried out a detailed multifunctional study of first-row transition-metal (Cr to Cu) nacnac imido and oxo complexes. In our opinion, two broad themes stand out from a plethora of detailed results.

First, all the imido and oxo species share essentially the same orbital ordering, which is $a_{1-2}(d_{\sigma}) \leq a_2(d_{\delta}) \leq a_{1-1}(d_{\sigma}) < b_2(d_{\pi}) < b_1(d_{\pi})$, which is in fact very similar to the orbital ordering in a simple (i.e., not particularly π -bonding) complex such as (nacnac)NiCl. This indicates that the orbital energy ordering is largely dictated by the trigonal-planar coordination environment rather than by the imido or oxo ligand. The remarkable stability of the d_{σ} orbitals, relative to the metal–imido linkage, owes largely to the way these orbitals can deform or hybridize as a result of the absence of ligands trans or equatorial with respect to the imido (or oxo) group. We believe that this is one of the first careful examinations of the “shape-shifting” nature of metal orbitals in low-coordinate environments.

Second, the pure functionals OLYP and OPBE, based on the Handy–Cohen OPTX exchange functional, appear to provide the best overall description of the spin-state energetics of the complexes examined. In particular, these two functionals correctly predict $S = 3/2$ and 0 ground states for the Fe(III) imido and Co(III) imido complexes, respectively. In contrast, classic pure functionals such as PW91 predict $S = 1/2$ ground states or at best equienergetic $S = 1/2$ and $3/2$ states for the Fe(III) imido complexes, while hybrid functionals predict $S = 1$ or 2 ground states for the Co(III) imido complexes, both of which are inconsistent with experimental results. In other words, there is no reason to suppose that hybrid functionals are inherently better than pure functionals, as is sometimes claimed.²⁶

Acknowledgment. This work was supported by the Research Council of Norway, the South African National Research Foundation (grant number 2054243), and the Central Research Fund of the University of the Free State, South Africa.

Supporting Information Available: Optimized PW91/TZP Cartesian coordinates for the molecules studied (67 pages). This information is available free of charge via the Internet at <http://pubs.acs.org>.

References

- (1) Nugent, W. A.; Mayer, J. M. *Metal–Ligand Multiple Bonds*; Wiley: New York, 1988.
- (2) Holm, R. H. *Chem. Rev.* **1987**, 97, 1401–1449.
- (3) Shan, X. P.; Que, L., Jr. *Inorg. Biochem.* **2006**, 100, 421–433.
- (4) Wigley, D. E. *Prog. Inorg. Chem.* **1994**, 42, 239–482.

- (5) Mehn, M. P.; Peters, J. C. *J. Inorg. Biochem.* **2006**, 100, 634–643.
- (6) For a representative review, see: Mindiola, D. J. *Acc. Chem. Res.* **2006**, 39, 813–821.
- (7) Mayer, J. M. *Comm. Inorg. Chem.* **1988**, 8, 125–135.
- (8) Hay-Motherwell, R. S.; Wilkinson, G.; Hussain-Bates, B.; Hursthouse, M. B. *J. Chem. Soc., Dalton Trans.* **1992**, 3477–3482.
- (9) Hay-Motherwell, R. S.; Wilkinson, G.; Hussain-Bates, B.; Hursthouse, M. B. *Polyhedron* **1999**, 12, 2009–2012.
- (10) Glueck, D. S.; Wu, J. X.; Hollander, F. J.; Bergman, R. G. *J. Am. Chem. Soc.* **1991**, 113, 2041–2054.
- (11) Glueck, D. S.; Green, J. C.; Michelman, R. I.; Wright, I. N. *Organometallics* **1992**, 11, 4221–4225.
- (12) Waterman, R.; Hillhouse, G. L. *Organometallics* **2003**, 22, 5182–5184.
- (13) Mindiola, D. J.; Hillhouse, G. L. *J. Am. Chem. Soc.* **2002**, 124, 9976–9977.
- (14) Melenkivitz, R.; Mindiola, D. J.; Hillhouse, G. L. *J. Am. Chem. Soc.* **2002**, 124, 3846–3847.
- (15) Mindiola, D. J.; Hillhouse, G. L. *J. Am. Chem. Soc.* **2001**, 123, 4623–4624.
- (16) Jenkins, D. M.; Betley, T. A.; Peters, J. C. *J. Am. Chem. Soc.* **2002**, 124, 11238–11239.
- (17) Shay, D. T.; Yap, G. P. A.; Zakharov, L. N.; Rheingold, A. L.; Theopold, K. H. *Angew. Chem., Int. Ed.* **2005**, 44, 1508–1510.
- (18) Hu, X.; Meyer, K. *J. Am. Chem. Soc.* **2004**, 126, 16322–16323.
- (19) Eckart, N. A.; Vaddadi, S.; Stoian, S.; Lachicotte, R. J.; Cundari, T. R.; Holland, P. L. *Angew. Chem., Int. Ed.* **2006**, 45, 6868–6871.
- (20) Dai, X.; Kapoor, P.; Warren, T. H. *J. Am. Chem. Soc.* **2004**, 126, 4798–4799.
- (21) Kogut, E.; Wiencko, H. L.; Cordeau, D. E.; Warren, T. H. *J. Am. Chem. Soc.* **2005**, 127, 11248–11249.
- (22) For a discussion of the spin-density profiles of various types of heme and nonheme Fe^{III/IV}/O species, see: Conradie, J.; Tangen, E.; Ghosh, A. *J. Inorg. Biochem.* **2006**, 100, 707–715.
- (23) For recent findings on iron-oxo spin-density profiles from our laboratory, see: (a) Ghosh, A.; Tangen, E.; Ryeng, H.; Taylor, P. R. *Eur. J. Inorg. Chem.* **2004**, 2442–2445. (b) Wasbotten, I.; Ghosh, A. *Inorg. Chem.* **2006**, 45, 4910–4913. (c) Conradie, J.; Wasbotten, I. H.; Ghosh, A. *J. Inorg. Biochem.* **2006**, 100, 502–506.
- (24) For a comparison of ab initio and DFT calculations on transition-metal spin-state energetics, see: Ghosh, A.; Taylor, P. R. *Curr. Opin. Chem. Biol.* **2003**, 91, 113–124.
- (25) For a series of commentaries on the performance of DFT on transition-metal complexes, see: Ghosh, A. *J. Biol. Inorg. Chem.* **2006**, 11, 671–673.
- (26) Ghosh, A. *J. Biol. Inorg. Chem.* **2006**, 11, 712–724.
- (27) Handy, N. C.; Cohen, A. *J. Mol. Phys.* **2001**, 99, 403–412.

- (28) Perdew, J. P.; Chevary, J. A.; Vosko, S. H.; Jackson, K. A.; Perderson, M. R.; Singh, D. J.; Fiolhais, C. *Phys. Rev. B: Condens. Matter Mater. Phys.* **1992**, *46*, 6671–6687.
- (29) Velde, G. T.; Bickelhaupt, F. M.; Baerends, E. J.; Guerra, C. F.; Van Gisbergen, S. J. A.; Snijders, J. G.; Ziegler, T. J. *J. Comput. Chem.* **2001**, *22*, 931–967.
- (30) Becke, A. D. *Phys. Rev. A: At., Mol., Opt. Phys.* **1998**, *38*, 3098–3100.
- (31) Lee, C.; Yang, W.; Parr, R. G. *Phys. Rev. B: Condens. Matter Mater. Phys.* **1988**, *37*, 785–789.
- (32) Becke, A. D. *Phys. Rev. A: At., Mol., Opt. Phys.* **1988**, *38*, 3098.
- (33) Perdew, J. P. *Phys. Rev. B: Condens. Matter Mater. Phys.* **1986**, *33*, 8822. Erratum: Perdew, J. P. *Phys. Rev. B: Condens. Matter Mater. Phys.* **1986**, *34*, 7406.
- (34) Perdew, J. P.; Burke, K.; Ernzerhof, M. *Phys. Rev. Lett.* **1996**, *77*, 3865–3868.
- (35) Perdew, J. P.; Burke, K.; Ernzerhof, M. *Phys. Rev. Lett.* **1997**, *78*, 1396.
- (36) Xu, X.; Goddard, W. A., III. *Proc. Natl. Acad. Sci. U.S.A.* **2004**, *101*, 2673.
- (37) Stephens, J.; Devlin, F. J.; Chabalowski, C. F.; Frisch, M. J. *J. Phys. Chem.* **1994**, *98*, 11623–11627.
- (38) Watson, M. A.; Handy, N. C.; Cohen, A. J. *J. Chem. Phys.* **2003**, *119*, 6475–6481.
- (39) Hertwig, R. H.; Koch, W. *Chem. Phys. Lett.* **1997**, *268*, 345–351.
- (40) Andres, H.; Bominaar, E. L.; Smith, J. M.; Eckert, N. A.; Holland, P. L.; Munck, E. *J. Am. Chem. Soc.* **2002**, *124*, 3012–3025.
- (41) Holland, P. L.; Cundari, T. R.; Perez, L. L.; Eckert, N. A.; Lachicotte, R. J. *J. Am. Chem. Soc.* **2002**, *124*, 14416–14424.
- (42) This is a simple C_{3v} model of a pseudotetrahedral Fe(III) trisphosphine imido complex reported in: Brown, S. D.; Betley, T. A.; Peters, J. C. *J. Am. Chem. Soc.* **2003**, *125*, 322–323.
- (43) Tangen, E.; Conradie, J.; Ghosh, A. *J. Chem. Theory Comput.* **2007**, *3*, 448–457.
- (44) For a recent review of bonding in NO complexes, see: Ghosh, A. *Acc. Chem. Res.* **2005**, *38*, 943–954.
- (45) Franz, K. J.; Lippard, S. J. *J. Am. Chem. Soc.* **1999**, *121*, 10504–10512.
- (46) Tangen, E.; Conradie, J.; Ghosh, A. *Inorg. Chem.* **2005**, *44*, 8699–8706.
- (47) Unusual d orbital hybridization also provides an explanation for the linearity of the NO group in the $S = 1/2$ $\{FeNO\}^7 [Fe(CN)_4(NO)]^{2-}$ anion: Conradie, J.; Ghosh, A. *J. Inorg. Biochem.* **2006**, *100*, 2069–2073.
- (48) In general, the great majority of the complexes studied conform to exact or approximately C_{2v} symmetry. The high-spin Fe(III) complexes are an exception; in these, the Fe–N_{imido} vector is somewhat bent to one side in the diketiminato plane. However, even in this case, the potential associated with the bending is very soft.
- (49) Tangen, E.; Ghosh, A. *J. Inorg. Biochem.* **2005**, *99*, 959–962.
- (50) We have observed a similar tendency of the PW91 functional to unduly favor low-spin states for a number of iron porphyrin complexes: (a) Ghosh, A.; Gonzalez, E.; Vangberg, T.; Taylor, P. *J. Porphyrins Phthalocyanines* **2001**, *5*, 345–356. (b) Ghosh, A.; Persson, B. J.; Taylor, P. R. *J. Biol. Inorg. Chem.* **2003**, *8*, 507–511. (c) Ghosh, A.; Taylor, P. R. *J. Chem. Theory Comput.* **2005**, *1*, 597–600.
- (51) There are few studies on the performance of the newer functionals vis-à-vis transition-metal spin-state energetics. However, the following papers, not necessarily concerned with transition metals, provide valuable evaluations of the OPTX-based functionals: (a) Vargas, A.; Zerara, M.; Krausz, E.; Hauser, A.; Daku, L. M. L. *J. Chem. Theory Comput.* **2006**, *2*, 1342–1359. (b) Ramachandran, B. *J. Phys. Chem. A* **2006**, *110*, 396–403. (c) Larkin, J. D.; Bock, C. W.; Schaefer, H. F., III. *J. Phys. Chem. A* **2005**, *109*, 10100–10105. (d) Xu, X.; Goddard, W. A., III. *J. Phys. Chem. A* **2004**, *108*, 8495–8504. (e) Guner, V. A.; Khuong, K. S.; Houk, K. N.; Chuma, A.; Pulay, P. *J. Phys. Chem. A* **2004**, *108*, 2959–2965.
- (52) Klinman, J. P. *Chem. Rev.* **1996**, *96*, 2541–2561.
- (53) Chen, P.; Solomon, E. I. *J. Am. Chem. Soc.* **2004**, *126*, 4991–5000.
- (54) Kamachi, T.; Shiota, Y.; Yoshizawa, K. *Inorg. Chem.* **2005**, *44*, 4226–4236.
- (55) Yoshizawa, K.; Kihara, N.; Kamachi, T.; Shiota, Y. *Inorg. Chem.* **2006**, *44*, 4226–4236.
- (56) Badiei, Y. M.; Krishnaswamy, A.; Melzer, M. M.; Warren, T. H. *J. Am. Chem. Soc.* **2006**, *128*, 15056–15057.
- (57) Spencer, D. J. E.; Reynolds, A. M.; Holland, P. L.; Jazdzewski, B. A.; Duboc-Toia, C.; Le Pape, L.; Yokota, S.; Tachi, Y.; Itoh, S.; Tolman, W. B. *Inorg. Chem.* **2002**, *41*, 6307–6321.

CT600337J